Available online at www.sciencedirect.com
ScienceDirect
Journal of the European Ceramic Society 29 (2009) 1053–1060
www.elsevier.com/locate/jeurceramsoc

Interaction of Al_2O_3-rich slag with MgO–C refractories during VOD refining—MgO and spinel layer formation at the slag/refractory interface

M. Guo *, S. Parada, P.T. Jones, E. Boydens, J.V. Dyck, B. Blanpain, P. Wollants

Department of Metallurgy and Materials Engineering (MTM), Katholieke Universiteit Leuven, Kasteelpark Arenberg 44, BE-3001 Leuven, Belgium

Received 5 June 2008; received in revised form 29 July 2008; accepted 31 July 2008
Available online 19 September 2008

Abstract

The interaction mechanisms between a pitch-bonded MgO–C refractory and an Al_2O_3 rich (~15 wt%) stainless steelmaking slag were investigated by rotating finger tests in a vacuum induction furnace. A porous MgO layer (instead of a dense MgO layer) was observed at the hot face of the MgO–C bricks. This implies that under the present low oxygen pressure conditions, the oxygen supply from the slag is insufficient to meet the demand of reoxidising the entire amount of Mg vapor generated from the MgO–C reaction to form a fully dense MgO layer. A $Mg(Al,Cr)_2O_4$ spinel layer with zoning was found at the slag/brick interface in the top slag zone specimen of Test 3 (CHS3). Based on the thermodynamic analyses with and experimental data, a mechanism of $Mg(Al,Cr)_2O_4$ spinel formation is proposed. Initially, hot face periclase grains take up Cr_2O_3, and to a much lesser extent, Al_2O_3 from the slag. The further diffusion of Cr_2O_3 and Al_2O_3 from the slag establishes a spinel layer of three distinct compositions of the type $MgAl_{2(1-x)}Cr_{2x}O_4$, with x decreasing when moving from the interior to the exterior spinel layer. Due to the low oxygen pressures, the thermodynamically less stable, dissolved Cr_2O_3 in the hot face periclase decomposes and forms chromium-rich metal droplets.

Keywords: Interaction mechanisms; MgO–C refractories; Steelmaking slags; MgO and spinel layers; Refractories

1. Introduction

MgO–C refractories have found widespread application in the steelmaking industry. The beneficial effects of the presence of carbon are explained by the following mechanisms: (a) carbon's non-wetting nature limiting slag penetration[1–3]; (b) a pressure build-up due to the evolution of carbon monoxide resisting slag and metal infiltration[4] and (c) formation of a dense MgO layer at the slag/brick interface physically preventing slag ingress.[5,6] The experimental results and theoretical analysis indicates that mechanism (c) is more likely in basic oxygen furnace (BOF) conditions.[7]

Kim and Lu[7] reported that formation of a dense MgO layer behind the hot face is the most likely explanation for the improved slag resistance of MgO–C BOF refractories. On the other hand, Baker et al.[8] pointed out that the conditions for formation of such a layer in the AOD (or VOD) process did not exist within the brick, owing to the low oxygen pressure in the system. Quon and Bell[9] conducted slag resistance tests on the MgO–C bricks with a carbon content of 15–24 wt% in vacuum at 1700 °C and stated that substantial MgO loss occurred in the brick due to the periclase grains being in contact with the carbon under vacuum conditions (reduction of MgO by carbon). No MgO dense layer at the slag/brick interface was observed in the tests leading to their conclusion that the gaseous Mg was completely removed under vacuum. This suggests that the sound performance of MgO–C bricks in primary steelmaking environments cannot be extrapolated to VOD refining. Nonetheless, the present authors[10] succeeded in partially extending the use of MgO–C bricks to the VOD process through industrial testing and *post mortem* assessments. However, two drawbacks should be highlighted. The industrial studies only investigated a VOD slag practice using Al_2O_3-poor $CaO–SiO_2–MgO–Al_2O_3$ (CSMA) slags (<8 wt% Al_2O_3). Secondly, a number of important parameters cannot be measured currently in the industrial environment, and it is practically impossible to extract the role of one specific parameter in industrial tests (e.g. Al_2O_3 level).

From a metallurgical point of view, Al_2O_3-rich $CaO–SiO_2–MgO–Al_2O_3$ (CSMA) slags would be beneficial to the desulphurisation process as elevated Al_2O_3 levels in the slag increase

* Corresponding author. Tel.: +32 16321183; fax: +32 16321991.
E-mail address: Muxing.Guo@mtm.kuleuven.be (M. Guo).

0955-2219/$ – see front matter © 2008 Elsevier Ltd. All rights reserved.
doi:10.1016/j.jeurceramsoc.2008.07.063

the lime solubility and sulphide capacity of the slag. Furthermore, an industrial observational study has suggested that higher Al_2O_3 levels may contribute a better chromium recovery during the reduction stage in the stainless steel EAF process and thus probably also in VOD refining.[11] However, the interaction between MgO–C refractories and Al_2O_3-rich CSMA VOD slags – which may influence the corrosion mechanisms of MgO–C refractories by direct or indirect dissolution of magnesia – has not been thoroughly studied.

In the present paper, rotating finger tests by a vacuum induction furnace simulating VOD process conditions were performed to investigate the interaction behavior between a pitch-bonded MgO–C and an Al_2O_3 rich (~15 wt%) stainless steelmaking slag. The possibility of forming a dense MgO layer behind the brick hot face under VOD conditions was experimentally studied. On the basis of the experimental observations and thermodynamic analyses, a formation mechanism for spinel layers at the slag/brick interface is proposed.

2. Experimental

2.1. Experimental conditions and procedure

Cylindrical refractory fingers (diameter 32; length 150 mm) were dipped into the corrosive slag and liquid stainless steel, and rotated for a certain number of cycles (rotation speed: 12 rpm). The experimental set-up and the detailed procedure have been reported in our previous work.[12] The experimental conditions are listed in Table 1. An alumina-chrome crucible (composition: 93 wt% Al_2O_3, 3.9 wt% Cr_2O_3; dimensions: Ø 175 mm × 220 mm) was used in the present tests resulting in high Al_2O_3 content slags. Approximately 15 kg of stainless steel (AISI 316), 1 kg of VOD-reduction slag (Table 2) supplied by a stainless steel company and a commercially available pitch-bonded MgO–C refractory were used in the tests. The chemical composition and physical properties of the MgO–C specimens are given in Table 3. To simulate the atmosphere in the VOD process, a gas mixture of CO and CO_2 was blown into the furnace at flowrates of 30 l/min CO and 1 l/min CO_2, controlled by mass-flow meters. The oxygen partial pressure was thus set to be $\sim 10^{-10}$ atm. Three tests were carried out at distinct temperatures (Tests 1 and 2: 1710 °C; Test 3: 1650 °C) with exposure times of 15, 35 and 45 min, respectively.

Temperature profile of the crucible with a charge of 15 kg stainless steel was measured in a separate melting test (Fig. 1), revealing that in the present experimental conditions, the temperature of the bottom slag zone was around 150 °C hotter than the top slag zone as the thickness of the slag zone was around 40 (see Fig. 1). The top and bottom slag zone correspond, respectively, to the gas/slag and slag/metal interface.

Table 2
Chemical compositions of the (as-delivered) VOD slag initially charged in the experiments as determined by ICP-AES (mass%)

MgO	Cr_2O_3	Al_2O_3	FeO	CaO	SiO_2	MnO	TiO_2
13.2	8.1	1.8	1.1	28	45	1.8	<0.5

Table 3
Chemical compositions and physical properties of pitch-bonded magnesia–carbon refractory finger specimens (as-delivered)

Chemical composition (in wt%)	Physical properties
92 MgO	Bulk density: 3.1 g/cm^3
5.5 C	Apparent porosity: 6.0 vol%
<1 SiO_2	Cold crushing strength: 40 N/mm^2
<0.7 Fe_2O_3	–

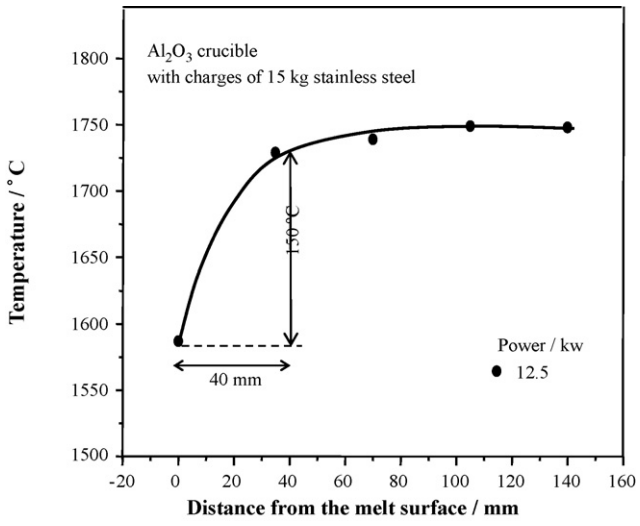

Fig. 1. Temperature profile of molten steel bath in the experiments.

2.2. Sample analysis techniques

The worn cylindrical refractory fingers were sliced into three pieces with a diamond saw. The slag zone sample was used for *post mortem* assessment. To evaluate the interaction behaviour in the different positions along the direction perpen-

Table 1
Experimental parameters and refractory materials for rotating finger tests in a vacuum induction furnace

Exp. no.	Time (min)	Temperature (°C)	P_{O_2} (atm)	Refractory materials	Others
Test 1	15	1710	4.28×10^{-10}		Steel mass: 15 kg Slag mass: 1 kg
Test 2	35	1710	4.28×10^{-10}	Pitch-bonded MgO–C	Rotating speed: 12 rpm Pressure: 500 Pa
Test 3	45	1650	1.48×10^{-10}		Sample size: Ø 32 mm × 150 mm

Table 4
Compositions of slag layer covered on the sample surface after completion of the test and composition of the infiltrated slag as determined by SEM-EDS (in wt%)

Sample	MgO	Al_2O_3	SiO_2	CaO	Cr_2O_3	C/S
CHS-1	21.0 ± 1.5	15.6 ± 1.4	29 ± 2	29 ± 2	5.4 ± 0.4	1.0
	–	–	–	–	–	–
CHM-1	–	–	–	–	–	–
	15.4 ± 0.5	*12.7 ± 0.6*	*33 ± 2*	*37 ± 3*	*1.2 ± 0.2*	*1.1*
CHS-2	18.5 ± 1.0	15.3 ± 1.0	30 ± 2	31 ± 1	4.5 ± 0.6	1.0
	21.6 ± 1.1	*10.0 ± 0.7*	*34 ± 1*	*33 ± 1*	*1.9 ± 0.1*	*1.0*
CHM-2	12.2 ± 1.0	14.8 ± 1.2	35 ± 2	35 ± 3	3.7 ± 0.4	1.0
	15.6 ± 1.4	*17.8 ± 1.5*	*33 ± 2*	*34 ± 1*	–	*1.0*
CHS-3	17.6 ± 0.7	12.0 ± 0.9	32 ± 2	34 ± 1	4.6 ± 0.3	1.1
	21.9 ± 2.0	*3.1 ± 0.3*	*37 ± 2*	*38 ± 2*	–	*1.0*
CHM-3	16.4 ± 0.3	13.1 ± 0.5	33 ± 2	35 ± 2	3.2 ± 0.9	1.1
	17.9 ± 1.1	*14.1 ± 1.2*	*36 ± 1*	*32 ± 1*	–	*0.9*

Data in italics: compositions of the infiltrated slag; values for MnO and FeO_x were constantly lower than 1 mass% and therefore not given here.

dicular to the slag surface, two specimens were prepared from all slag zone samples. These consisted of the cross section at the top (CHS) and the bottom (CHM) part of the slag zone. The details of analysis techniques, including semi-quantitative SEM-EDS analyses[12] and electron probe micro analysis (EPMA) EDS analyses[10] and slag analysis with inductively coupled plasma atomic emission spectroscopy (ICP-AES),[13] have been given in previous work. Slags attached to the refractory specimens surface and those infiltrated into bricks were measured with semi-quantitative SEM-EDS analyses (Table 4). The results were obtained from at least four global analyses of the slag areas (selected scans covering ~2500 μm^2 per analysis).

3. Results and discussions

3.1. General overview of the MgO–C refractory/slag interface

Fig. 2 shows a general overview of the MgO–C refractory/slag interface after the experiments. SEM observation of the interfaces reveals: (1) Removal of carbon by direct carbon burnout did not occur due to the low oxygen partial pressure during the tests. Therefore, no decarburized zone existed at the refractory hot face limiting excessive slag infiltration, particularly for the top slag zone samples (see Fig. 2(a), (c) and (e)). (2) Slag penetration took place along the intragranular periclase grain boundaries and open pores or cracks in the bricks. Temperature and exposure time substantially affected the infiltration level, i.e. higher test temperatures and longer interaction times gave rise to a more severe slag infiltration (see Fig. 2(d), slag penetrated throughout the samples). (3) The presence of the irregular shape of metallic particles mainly in contact with carbon at the slag/brick interface corroborated the occurrence of carbon oxidation by slags (Fig. 2(c), (e) and (f)). (4) The rough brick surface, which was observed in the bottom slag zone specimens (Fig. 2(b), (d) and (f)), indicated a substantial erosion of the periclase grains in the vicinity of the brick hot face. This is believed to be the result of the combined effect of high temperature (Fig. 1: higher temperature at bottom slag zone than at top slag zone) softening of any intragranular silicate bond, and the strong stirring at the slag/metal interface caused by the metal induction leading to further erosion. (5) An almost continuous MgO layer formed at the hot face in the bottom slag zone specimen of Test 1 (Fig. 2(b)) and Test 2 (Fig. 2(d)). Instead of a dense MgO layer, a porous layer (see high magnification image from Fig. 3) was observed consisting of a large number of fine MgO grains (5–50 μm) with a slag matrix. Little covering slag layer was observed on the sample surface, presumably because of the lower slag viscosity at higher temperatures (1710 °C). (6) A thin (20–50 μm) spinel layer (position A in Fig. 2(e), see its high magnification image from Fig. 4) was found at the slag/brick interface in the top slag zone specimen of Test 3 (CHS3), probably due to the lowest temperature for this specimen. Mechanisms for formation of the porous MgO layer and of the spinel layer are discussed in the following sections.

3.2. Formation of a MgO layer

A number of studies[5,6,14] have indicated the beneficial protective effect of the MgO dense layer formed at the hot face of MgO–C bricks. This layer arises from the reduction of MgO by C to Mg vapor that is transported to the hot face where it is subsequently re-oxidized by oxygen in the atmosphere and/or by the oxidation of slag to fine grained dense MgO helping to prevent slag/metal ingress. The experimental observation verified that the reduction of MgO by C within the MgO–C bricks occurred under the present test conditions. During the tests, a substantial volume of Mg vapor condensed as MgO in the cooler parts of the vacuum chamber, suggesting MgO loss occurred in the bricks due to reaction (1):

$$MgO(s) + C(s) = Mg(g) + CO(g) \quad (1)$$

Fig. 2(b) and (d) clearly shows that MgO layer formed at the hot face for the samples of Tests 1 and 2 in the bottom slag zone

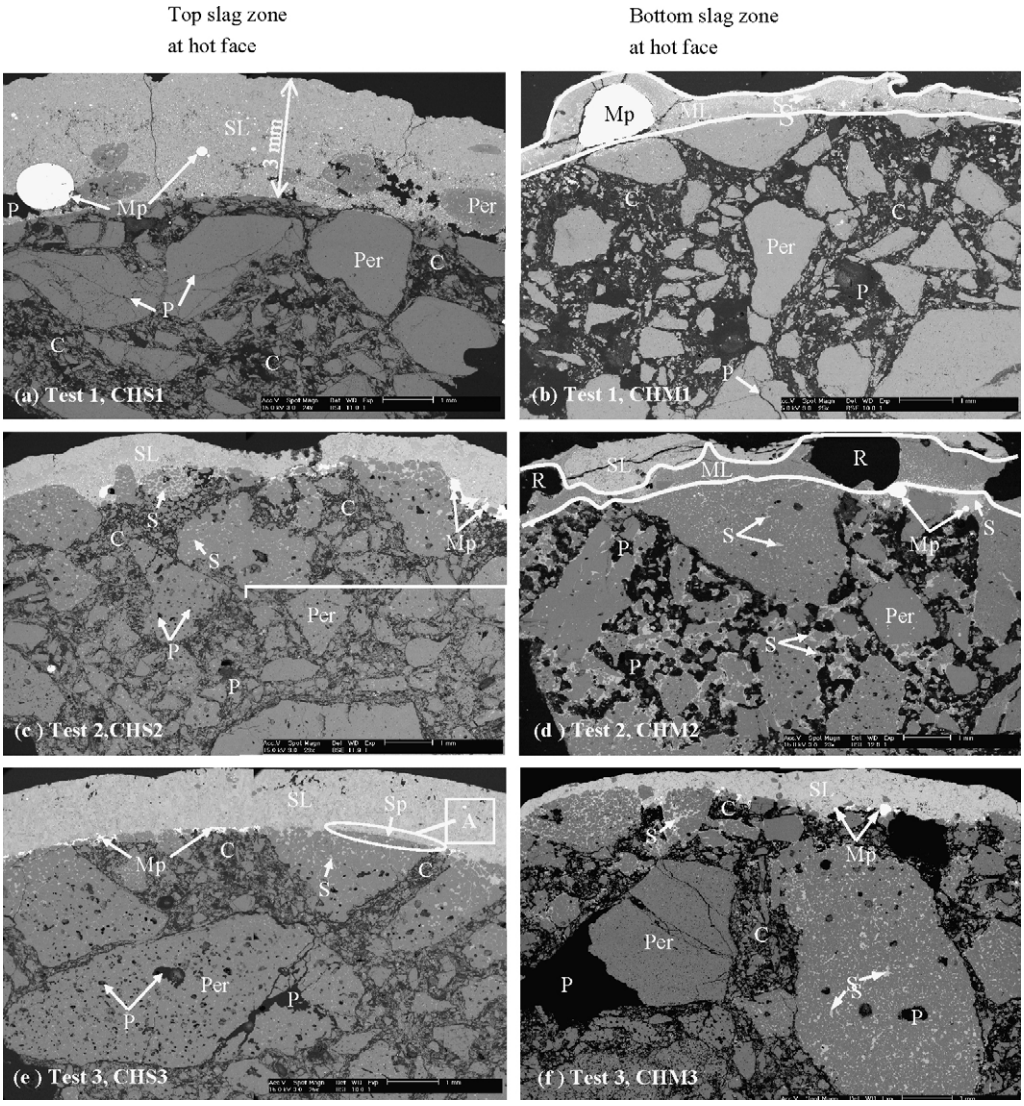

Fig. 2. Overview of worn samples of Tests 1, 2 and 3, showing the hot face at the top (CHS1, 2 and 3) and bottom (CHM1, 2 and 3) slag zone: Per = magnesia (periclase); C = carbon; S = infiltrated slag; SL = slag layer; ML = MgO layer; Mp = metallic particle; P = pore or crack; Sp = spinel layer (see Fig. 4, the high magnification image of position A); R = resin.

position. Baker et al.,[8] however, reported that the conditions for formation of this layer did not exist within the bricks in VOD or AOD environment due to the low oxygen atmosphere, which was similar with the present experimental conditions. However, it is not surprising that oxygen can be supplied from the slag to the hot face through the reducible components in slag (e.g. Cr_2O_3, MnO and FeO), thus helping the reoxidation of magnesium vapor to MgO at the hot face, while causing precipitation of metallic particles. This can be expressed by the following reactions:

$$3Mg(g) + (Cr_2O_3)_{slag} = 3MgO(s) + 2[Cr]_{metal} \quad (2)$$

$$Mg(g) + (MnO)_{slag} = MgO(s) + [Mn]_{metal} \quad (3)$$

$$Mg(g) + (FeO)_{slag} = MgO(s) + [Fe]_{metal} \quad (4)$$

High magnification images (Fig. 3) of the MgO layers from Fig. 2(b) and (d), confirmed the above explanation. Fig. 3 shows, rather than a dense MgO layer, a porous MgO layer consisting of fine MgO grains and small (0.5–10 μm) metal particles (EDS analysis: 30–57 wt% Cr, 43–70 wt% Fe, 0–1.1 wt% Mn) was present at grain boundaries within the slag matrix. Compositional analyses by SEM-EDS indicate that the slag matrix is depleted in Cr_2O_3, MnO and FeO (Table 5). Furthermore, growth of these fine MgO grains with reaction time was clearly observed as depicted in Fig. 3(a) and (b). As the holding time was increased from 15 (Test 1) to 35 min (Test 2), the fine MgO grains dispersed in the slag matrix coarsen and merge, leaving less slag matrix and resulting in a larger (~10 μm) metal particles at the MgO grain boundaries. Content changes of Cr_2O_3, MnO and FeO (with time, Table 5) in the slag between the fine MgO grains further indicate MgO formation through the reoxidation of Mg vapor by reducible slag components (e.g. Cr_2O_3, MnO and FeO). The formation of this porous MgO layer at the refractory hot face implies that, under the present low oxygen pressure condition, the oxygen level supplied through the slag is insufficient to meet the demand of re-oxidising the entire volume of Mg vapor gen-

Table 5
Compositions of slag between the fine MgO grains in loose MgO layer (in wt%), as determined by SEM-EDS

Sample	Test condition	MgO	Al_2O_3	SiO_2	CaO	Cr_2O_3	MnO	FeO
Initial slag	1710 °C, 0 min	13.2 ± 0.8	1.8 ± 0.1	45 ± 2	28 ± 1	8.1 ± 1.0	1.8 ± 0.2	1.1 ± 0.1
CHM1	1710 °C, 15 min	13.9 ± 1.0	15.5 ± 0.5	31 ± 1	37 ± 1	1.2 ± 0.1	1.1 ± 0.1	<0.5
CHM2	1710 °C, 35 min	13.1 ± 0.9	13.7 ± 0.7	35 ± 2	38 ± 2	<0.5	<0.5	<0.5

erated from the MgO–C reaction (Eq. (1)) to form a dense MgO layer. As calculated by Kim and Lu,[7] the rate of the dense MgO layer formation increases with temperature. This is probably the predominant reason why the MgO layers were found only in the bottom slag zone specimens (with higher temperature) of Tests 1 and 2 (Fig. 2(b) and (d)). Obviously, the formation and destruction of the MgO layer may be caused by a number of factors (e.g. oxygen pressure, temperature, slag composition) and careful control of conditions both inside and outside the refractory are required to maintain the delicate balance between dense layer dissolution and formation.[15] Due to the fragile character of this MgO layer, it is speculated that it would not withstand the turbulent conditions in the VOD process. Although it may form thermodynamically, kinetic and mechanical aspects would thus render it ineffective in the industrial application.

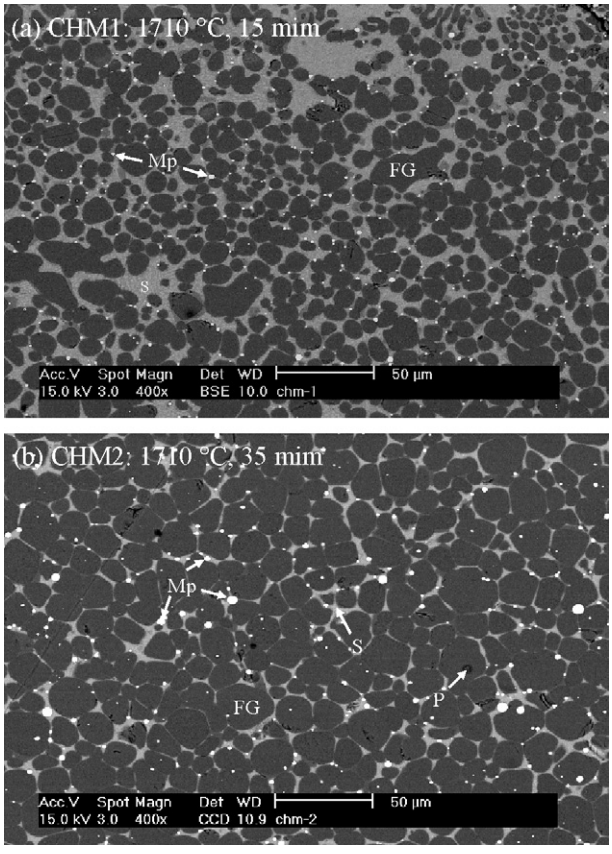

Fig. 3. Higher magnification images of MgO layer also shown in (a) Fig. 2(b) and (b) in Fig. 2(d), showing a porous layer of fine MgO grains with small metal particles located at grain boundaries and a slag depleted in iron and chromium oxides: FG = fine MgO grain; S = slag; Mp = metal particle; P = pore or crack.

3.3. Formation of a spinel layer

Fig. 4 shows a dense spinel layer with variable compositions at the slag/brick interface. The occurrence of this spinel layer could imply a lower wear rate of the MgO–C bricks in the slagline, possibly enhancing their overall performance. However, only at the slag/brick interface in the top slag zone specimen of Test 3 (CHS3) was such a solid spinel layer (20–40 μm thick) found (Fig. 4). As the final slag composition (Al_2O_3 and Cr_2O_3 content and C/S ratio, see Table 4) was almost identical for the different tests, this implies that temperature (apart from time) was the only variable parameter. The lower the temperature, the more prone to spinel precipitation at the interface for the MgO, Al_2O_3 and Cr_2O_3 saturated slag. Taking the vertical temperature gradient over the refractory fingers into account (Fig. 1), the temperature of the CHS3 sample can be estimated to be in the vicinity of 1500 °C, while that of CHS1 and CHS2 was approximately 1560 °C. In the two latter samples, the spinel layer was not formed. The same is valid for the (warmer) bottom slag zone specimens (CHM1, 2 and 3).

3.3.1. Composition of the spinel layer

Semi-quantitative analyses of the spinel layer in CHS3 shows that it is $Mg(Al,Cr)_2O_4$ spinel composed of approximately 46–69 wt% Al_2O_3 with 24–25 wt% MgO and 5–30 wt% Cr_2O_3 as demonstrated in Table 6. X-ray line analyses of the spinel layer (Fig. 5) reveal that the MgO content across the spinel layer remains unaltered while the Cr_2O_3 content substantially

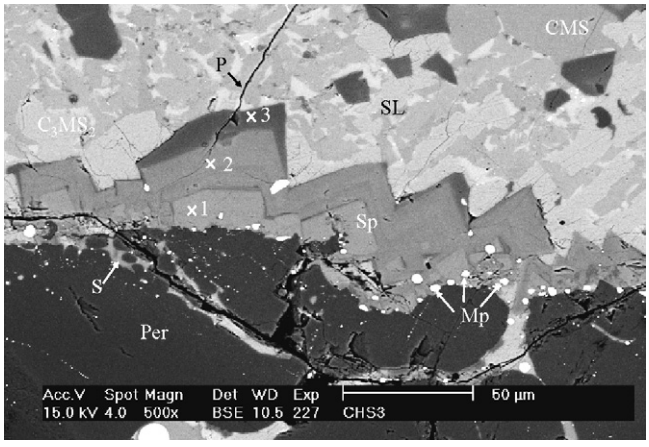

Fig. 4. BSE electron images of (Mg) $(Cr,Al)_2O_4$ spinel layer formed at slag/refractory interface for the sample of CHS3 (high magnification images of the position A in Fig. 2(e)): Per = periclase; S = infiltrated slag; Mp = precipitate of Cr-rich metal; SL = slag layer; Sp = spinel layer; CMS = $CaO{\cdot}MgO{\cdot}SiO_2$; C_3MS_2 = $3CaO{\cdot}MgO{\cdot}2SiO_2$; 1, 2 and 3 = spinel phases with different compositions as shown in Table 6.

Table 6
Three distinct compositions of the type $MgAl_{2(1-x)}Cr_{2x}O_4$ spinels, with x decreasing when moving away from the interior to the exterior spinel layer (in Fig. 4), as determined by SEM-EDS (in wt%)

Phases	MgO	Al_2O_3	Cr_2O_3	X
1	24 (48)	46 (37)	30 (16)	0.30
2	24 (47)	51 (40)	25 (13)	0.24
3	26 (48)	69 (50)	5.0 (2.4)	0.05

Unit between ( ): at%.

increases with a simultaneous decrease in the Al_2O_3 level closer to the magnesia refractory surface (along the path A–B). The chromium-rich metal particles in Figs. 4 and 5, on the other hand, are the result of decomposition of Cr_2O_3 both in the hot face periclase solid solution and in the spinel layer. This is a phenomenon that is caused by the low oxygen pressure ($\sim 10^{-10}$ atm) and high temperature conditions.

3.3.2. Thermodynamic considerations

The formation of $Mg(Al,Cr)_2O_4$ spinel on periclase, when periclase is in contact with a CSMA slags, can be represented by the reactions

$$MgO(s) + (Al_2O_3) = MgAl_2O_4(s) \quad (5)$$

$$MgO(s) + (Cr_2O_3) = MgCr_2O_4(s) \quad (6)$$

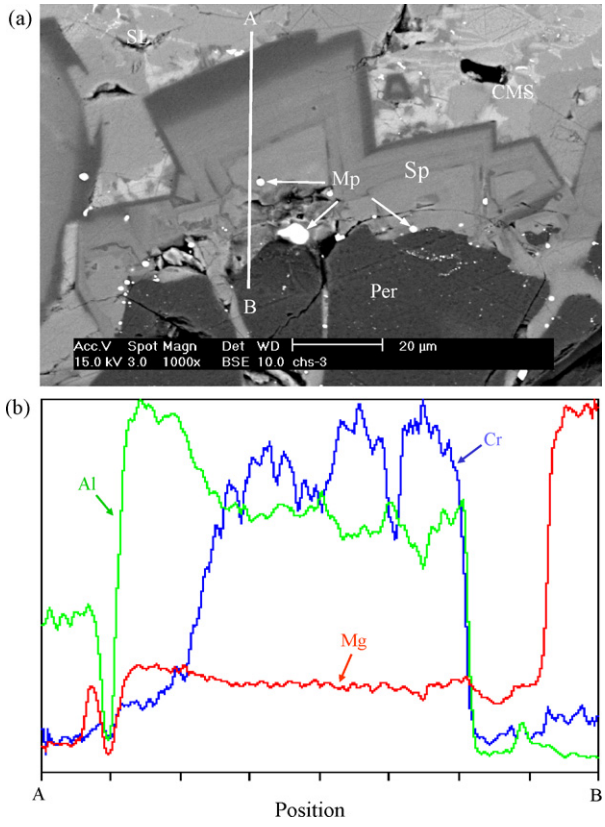

Fig. 5. X-ray line analyses of the spinel layer at slag/brick interface: (a) BSE image of (Mg) $(Cr,Al)_2O_4$ spinel layer at slag/brick interface, (b) concentration profiles along the line A–B in (a) BSE image: Per = periclase; slag; Mp = precipitate of Cr-rich metal; SL = slag layer; Sp = spinel layer; CMS = $CaO{\cdot}MgO{\cdot}SiO_2$.

where parentheses indicate a species dissolved in the slags. The Gibbs free energy changes for reactions (5) and (6) therefore can be calculated by Eqs. (7) and (8):

$$\Delta G_5 = \Delta G_5^0 + RT \ln \frac{a_{MgAl_2O_4}}{a_{MgO}{\cdot}a_{Al_2O_3}} \quad (7)$$

$$\Delta G_6 = \Delta G_6^0 + RT \ln \frac{a_{MgCr_2O_4}}{a_{MgO}{\cdot}a_{Cr_2O_3}} \quad (8)$$

where a_i is the thermodynamic activity of species i, ΔG_5^0 and ΔG_6^0 are the standard Gibbs free energy changes for reactions (5) and (6), respectively. The standard states for MgO, Al_2O_3 and Cr_2O_3 are taken herein as the pure solids at the temperature of interest and the standard states for $MgAl_2O_4$ and $MgCr_2O_4$ are taken as $MgAl_2O_4$ and $MgCr_2O_4$ saturated with respect to periclase (MgO) at the temperature of interest. When $MgAl_2O_4$ and/or $MgCr_2O_4$ nucleate on periclase $MgAl_2O_4$ and/or $MgCr_2O_4$ are saturated with respect to MgO. Therefore, the activities of both $MgAl_2O_4$ and $MgCr_2O_4$ spinels can be set equal to 1. The value of Al_2O_3 activity in CSMA slag can be estimated by Eq. (9)[16]:

$$\log a_{Al_2O_3} = \frac{-0.275(\text{mass\% CaO}) + 0.167(\text{mass\% MgO})}{(\text{mass\% SiO}_2) - 0.03(\text{mass\% Al}_2\text{O}_3) - 1.56} \quad (\text{the correlation coefficient } R = 0.89) \quad (9)$$

By substituting the covered slag compositions of Test 3 (Table 4, sample CHS3) into Eq. (9), $a_{Al_2O_3}$ was calculated to be 0.26. Taking the covered slag composition of sample CHS3 (C/S ratio = 1.1 and Cr_2O_3 = 4.6 mass%) and the experimental atmosphere (($P_{O_2} = 1.48 \times 10^{-10}$ atm) into account, the data for the activity of Cr_2O_3 in the slag was estimated as 0.35 according to the measurements by Morita et al.[17] The standard free energies were obtained from Rein and Chipman[18] for ΔG_5^0 ($\Delta G_5^0 = -18,800 - 6.3T$ J/mol), from Tretjakow and Schmalzried[19] for ΔG_6^0 ($\Delta G_6^0 = -42,929 + 7.1T$ J/mol), respectively yielding the values of $\Delta G_5^0 = -29,970$ J/mol and $\Delta G_6^0 = -30,340$ J/mol at 1500 °C (the estimated temperature for the sample CHS3). Substitutions of the standard free energy (ΔG_5^0 and ΔG_6^0) and activity (a_{MgO}, $a_{MgAl_2O_4}$, $a_{MgCr_2O_4}$, $a_{Al_2O_3}$ and $a_{Cr_2O_3}$) values quoted above into Eqs. (7) and (8), give the values of the Gibbs free energy changes at 1500 °C for reactions (5) and (6) as, respectively, $\Delta G_5 = -10,123$ J/mol and $\Delta G_6 = -15,167$ J/mol. Accordingly, it can be concluded that the thermodynamic criterion for the formation of both $MgAl_2O_4$ (Eq. (5)) and $MgCr_2O_4$ (Eq. (6)) spinels on periclase surface at 1500 °C (which was the estimated temperature of Test 3 for top slag zone sample, CHS3) was satisfied. These were in agreement with the present experimental observations, in which the $Mg(Al,Cr)_2O_4$ spinels were detected on the refractory hot face.

3.3.3. Formation mechanism of the zoning spinel layer

High-temperature dissolution of refractory into slag can be direct or indirect, depending on whether or not a solid compound (e.g. spinel) layer forms at brick/slag interface.[20] Formation of CA_6 and hercynitic spinel layers was observed at alumina/silicate slag (iron-containing) interfaces.[21,22] On the

other hand, Zhang and Lee[23] reported that the dissolution of magnesia into EAF model slag is essentially indirect due to the formation of magnesiowustite layer between MgO and slag. Similarly, a zoning spinel layer was detected in the present work. According to the compositional analysis results with respect to the zoning spinel (Fig. 4), periclase grains and the slag attached on the sample, mechanisms of the zoning spinel formation on the hot face periclase grains are proposed as follows.

Initially, magnesia grains take up Cr_2O_3 from the slag to form a periclase solid solution. Al_2O_3 also dissolves in magnesia, albeit to a much lower extent due to the lower affinity of magnesia for Al_2O_3 (higher binding energy of MgO with Cr_2O_3 than with Al_2O_3).[24] Table 7 shows that the periclase solid solution with approximately 3–5 mass% Cr_2O_3 and 0 to 3 mass% Al_2O_3 is in contact with the spinel layer. Homer and Richardson[25] studied the reaction of synthetic spinels with magnesia at high temperature and found that very little Cr^{3+} diffuses out from the spinel ($MgCr_2O_4$) to the MgO. Therefore, the dissolved Cr_2O_3 and Al_2O_3 (in the periclase grains) would arise from the diffusion of Cr_2O_3 and Al_2O_3 from the slag in contact with the periclase grains prior to the spinel formation. Once the solubility limit of Cr_2O_3 in the periclase is exceeded Cr_2O_3 starts to forms a separate compound (Cr_2O_3·MgO spinel) with MgO, owing to the stronger affinity of MgO for Cr_2O_3 than for Al_2O_3 at the present elevated temperature (see the values of ΔG_5 and ΔG_6). On the other hand, because of the lower solubility of Al_2O_3 in magnesia (Table 7) and a negative Gibbs free energy change of Eq. (5) (ΔG_5), an Al_2O_3·MgO spinel can also be formed immediately when it is in contact with MgO. Furthermore, since the periclase grains took up much more Cr_2O_3 than Al_2O_3 from the slag and the originally higher content of Al_2O_3 than that of Cr_2O_3 in the slag (see Table 4), the slag in contact with the periclase is richer in Al_2O_3 with reference to Cr_2O_3. The first spinel (Fig. 4, spinel phase 1) formed will, therefore, not only contain Cr_2O_3 but also Al_2O_3, i.e. $MgAl_{2(1-x)}Cr_{2x}O_4$—as described in reaction (10):

$$\mathrm{MgO(s)} + (1-x)(\mathrm{Al_2O_3})_{\mathrm{slag}} + x(\mathrm{Cr_2O_3})_{\mathrm{slag}} = \mathrm{MgAl_{2(1-x)}Cr_{2x}O_4} \quad \text{with } x = 0.30\ (\text{Table6, spinel phase 1}) \tag{10}$$

The further supply of additional Al_2O_3 from the slag, with respect to a limited Cr_2O_3 supply, results in the formation of a second spinel (Fig. 4, spinel phase 2) that is richer in aluminium with respect to the first one, as shown in reaction

Table 7
Compositions of the periclase solid solution in contact with spinel layer, as determined by EPMA (in wt%)

Points	MgO	Al_2O_3	Cr_2O_3	FeO	MnO
1	90.1	2.1	5.3	0.3	0.9
2	92.9	2.5	3.0	0.1	0.8
3	95.1	1.0	3.2	0.0	0.6
4	93.3	2.0	3.5	0.0	0.9
5	95.2	0.0	3.6	0.0	0.9

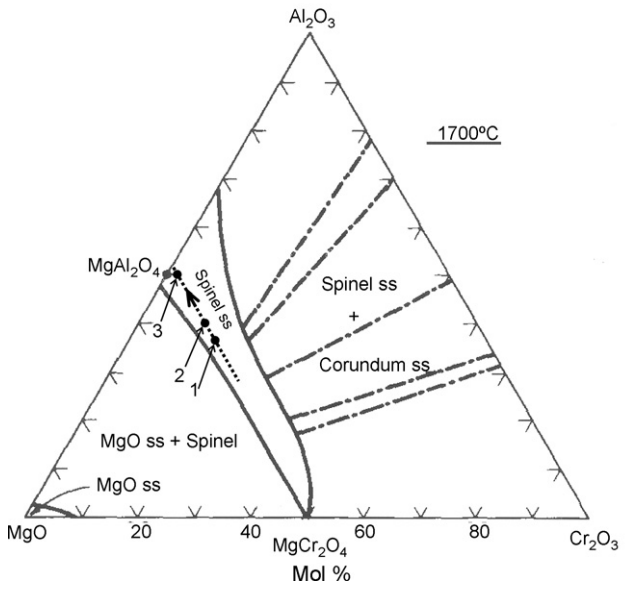

Fig. 6. The system MgO–Al_2O_3–Cr_2O_3, isothermal section at 1700 ± 15 °C. Dash-dot lines are tie lines between the corundum and spinel solid solutions; solid dot (●) the compositions of spinel numbers 1, 2 and 3 in the corresponding spinel zone in Fig. 4; dotted-line with arrow shows evolution of spinel compositions during its formation at 1500 °C for the sample CHS3.

(11):

$$\mathrm{MgO(s)} + (1-x)(\mathrm{Al_2O_3})_{\mathrm{slag}} + x(\mathrm{Cr_2O_3})_{\mathrm{slag}} = \mathrm{MgAl_{2(1-x)}Cr_{2x}O_4} \quad \text{with } x = 0.24\ (\text{Table6, spinel phase 2}) \tag{11}$$

The local slag composition is now strongly impoverished in Cr_2O_3 which is the result of its local absorption into the periclase solid solution and into the two former spinels. Subsequently, an external third spinel may be formed. SEM-EDS analyses reveal that this is almost pure MA spinel (see Table 6, spinel phase 3, $MgAl_{2(1-x)}Cr_{2x}O_4$ with $x = 0.05$). On the other hand, ions of Cr^{3+} dissolved in the hot face of periclase grains and in the spinel are decomposed to the metallic state (see Fig. 4) because of the low oxygen pressure conditions (10^{-10} atm).

Formation of the zoning spinel with three different compositions (Fig. 4) can be further understood through the MgO–Al_2O_3–Cr_2O_3 diagram (1700 °C, see Fig. 6).[26] Note that in the present specimen (CHS3) the estimated temperature is approximately 1500 °C, at which the single spinel solid solution region in the MgO–Al_2O_3–Cr_2O_3 phase diagram could be narrower than at 1700 °C. SEM-EDS analyses (Table 6) are marked in Fig. 6 and illustrate the evolution of the spinel composition along the layer from the interior to the exterior spinel. The first spinel type is rich in Cr_2O_3 (Point 1). This spinel, which is in equilibrium with the periclase solid solution grains (composition in mass%: 95–97 MgO; 3–5Cr_2O_3; 0–3 Al_2O_3), consumes a lot of Cr_2O_3 from the slag so that the local Cr_2O_3/Al_2O_3 ratio in the slag in contact with the formed first spinel decreases. Therefore, further spinel formation can only proceed with higher Al_2O_3 compositions (Point 2) up to nearly pure $MgAl_2O_4$ (Point 3).

However, to attain a complete understanding of these complex phenomena, further kinetic considerations need to be considered.

4. Conclusions

The contribution of the external oxygen source (from atmosphere and/or slag) to the decarburization of the MgO–C refractory was limited under the present test conditions. Indirect oxidation of carbon by the MgO–C reaction in the bulk of the brick was the main decarburization mechanism.

The erosion of the periclase grains from the brick surface to the slag phase occurred in the bottom slag zone specimens, owing to the high temperature softening of any intragranular silicate bond and strong agitation at the slag/metal interface caused by the metal induction.

A porous MgO layer (instead of a dense MgO layer) was formed at the hot face of the MgO–C bricks. This implies that under the present low oxygen pressure conditions, the oxygen supply from the slag is insufficient to meet the demand of reoxidising the entire volume of Mg vapor generated from the MgO–C reaction to form a really dense MgO layer. Under industrial and turbulent conditions, the present MgO layer would presumably be ineffective in retarding slag infiltration.

A spinel layer with zoning was observed at the slag/brick interface in the top slag zone specimen of Test 3 (CHS3). Thermodynamic calculation with respect to the Gibbs free energy change for the formation of $Mg(Al,Cr)_2O_4$ spinels has confirmed the interpretation present experimental observation.

Based on the compositional analysis results, a formation mechanism for formation of the zoning spinel layer is proposed. Initially, hot face periclase grains dissolve (or take up) Cr_2O_3, and to a much lesser extent, Al_2O_3 from the slag to form periclase solid solution. Once the solubility limits of Cr_2O_3 and Al_2O_3 in the periclase are exceeded, further diffusion of Cr_2O_3 and Al_2O_3 from the slag establishes a spinel layer of three distinct compositions of the type $MgAl_{2(1-x)}Cr_{2x}O_4$ spinel, with x decreasing on moving from the interior to the exterior spinel layer. Due to the low oxygen pressures, the thermodynamically less stable, dissolved Cr_2O_3 in the hot face periclase decomposes and forms chromium-rich metal droplets. To further assess the conditions for the spinel formation and its industrial relevance, further kinetic studies are required.

Acknowledgements

This work was performed with the financial and technical support of U&A Belgium and the IWT (project no. 990348). The authors are grateful to the engineers of U&A Belgium and PVA for their close co-operation with our team. Practical advice from Heraeus Electro-Nite and Jacques Cortier (Dyson Refractories) was much appreciated.

References

1. Barthel, H., Effect of carbon in tar-impregnated burnt magnesite bricks on the wear of basic oxygen furnace linings. *Stahl U. Eisen*, 1966, **86**, 81–88.
2. Limes, R. W., Refractories for basic oxygen furnace. *J. Met.*, 1966, 865–869.
3. Herron, R. H., Beechan, C. R. and Padfield, R. C., Slag attack on carbon-bearing basic refractories. *Am. Ceram. Soc. Bull.*, 1967, **46**, 1163–1168.
4. Robinson, P. C., Some observation on unused and used refractories from oxygen steelmaking vessels. *J. Refract.*, 1966, **42**, 218–222.
5. Pickering, G. D. and Batchelor, J. D., Carbon–MgO reactions in BOF refractories. *Am. Ceram. Soc. Bull.*, 1971, **50**, 611–614.
6. Leonard, R. J. and Herron, R. H., Significance of oxidation–reduction reactions within BOF refractories. *J. Am. Ceram. Soc.*, 1972, **55**, 1–6.
7. Kim, S. M. and Lu, W. K., Kinetics and mechanism of the formation of dense MgO layer in pitch-bearing magnesite brick during service. *Met. Trans.*, 1978, **9B**, 353–364.
8. Baker, B. H., Brezny, B. and Shultz, R. L., The role of carbon in MgO refractories. *Am. Ceram. Soc. Bull.*, 1975, **54**, 665–666.
9. Quon, D. H. and Bell, K. E., Performance of magnesia–carbon bricks in vacuum at high temperature. *J. Can. Ceram. Soc.*, 1987, **56**, 39–44.
10. Smets, S., Parada, S., Weytjens, J., Heylen, G., Jones, P. T., Guo, M. *et al.*, Behaviour of magnesia–carbon refractories in vacuum-oxygen decarburization ladle linings. *Ironmaking Steelmaking*, 2003, **30**, 293–300.
11. Guo, M., Durinck, D., Jones, P. T., Heylen, G., Hendrickx, R., Baeten, R. *et al.*, EAF stainless steel refining—Part I: Observational study on chromium recovery in an eccentric bottom tapping furnace and a spout tapping furnace. *Steel Res. Int.*, 2007, **78**(2), 117–124.
12. Guo, M., Parada, S., Smets, S., Jones, P. T., Van Dyck, J., Blanpain, B. *et al.*, Laboratory study of the interaction mechanisms between magnesia–chromite refractories and Al_2O_3-rich VOD slags. In *Proceedings of 7th International Conference on Molten Slags, Fluxes and Salts*, 2004, pp. 327–336.
13. Jones, P. T., Hermans, P., Blanpain, B. and Wollants, P., Optimization of an accurate and precise analysis procedure for metallurgical VOD slags with ICP-OES. *Atom. Spectrosc.*, 2000, **21**, 86–92.
14. Brezny, B. and Landy, R. A., Microstructural and chemical changes of pitch impregnated magnesite brick under reducing conditions. *Trans. J. Br. Ceram. Soc.*, 1972, **71**, 163–170.
15. Lee, W. E. and Zhang, S., Melt corrosion of oxide and oxide–carbon refractories. *Int. Mater. Rev.*, 1999, **44**, 77–104.
16. Ohta, H. and Suito, H., Activities of SiO_2 and Al_2O_3 and activity coefficients of Fe_tO and MnO in CaO–SiO_2–Al_2O_3–MgO slags. *Metall. Trans. B*, 1998, **29B**, 119–129.
17. Morita, K., Mori, M., Guo, M., Ikagawa, T. and Sano, N., Activity of chromium oxide and phase relations for the CaO–SiO_2–CrO_x system at 1873 K under moderately reducing conditions. *Steel Res.*, 1999, **70**, 319–324.
18. Rein, R. H. and Chipman, J., Activity in the liquid solution SiO_2–CaO–MgO–Al_2O_3 at 1600 °C. *Trans. TMS-AIME*, 1965, **233**, 415–425.
19. Tretjakow, J. D. and Schmalzried, H., Thermodynamics of spinel phases. *Ber. Bunsengesellsch*, 1966, **69**, 396–402.
20. Lee, W. E., Zhang, S., Marriott, N. J. and Sarpoolaky, H., Influence of microstructure on refractories corrosion. In *Proceedings of the United Int. Tech. Conf. on 'Refractories' (UNITECR'01)*, 2001, pp. 1321–1329.
21. Zhang, S., Rezaie, H. R., Sarpoolaky, H. and Lee, W. E., Alumina dissolution into silicate slag. *J. Am. Ceram. Soc.*, 2000, **83**(4), 897–930.
22. Sarpoolaky, H., Zhang, S. and Lee, W. E., Corrosion of high alumina and near stoichiometric spinels in iron-containing silicate slags. *J. Eur. Ceram. Soc.*, 2003, **23**(2), 293–300.
23. Zhang, S., Sarpoolaky, H., Marriott, N. J. and Lee, W. E., Penetration and corrosion of magnesia grain by silicate slags. *Br. Ceram. Trans.*, 2000, **99**(6), 248–255.
24. Jung, I. H., Decterov, S. and Plton, A. D., Thermodynamic modelling of MgO–Al_2O_3–CrO–Cr_2O_3 systems. *J. Am. Ceram. Soc.*, 2005, **88**(7), 1921–1928.
25. Homer, P. N. and Richardson, H. M., The reaction of some synthetic spinels with magnesia at high temperatures. *Trans. Br. Ceram. Soc.*, 1964, **63**, 389–415.
26. Greskovich, C. and Stubican, V. S., Coherent precipitation in the system MgO–Al_2O_3–Cr_2O_3. *J. Am. Ceram. Soc.*, 1968, **51**, 42–46.